Journal of Nanoparticle Research (2007) 9:1097–1107
DOI 10.1007/s11051-006-9204-4

Sinter-active nanocrystalline CeO_2 powder prepared by a mixed fuel process: Effect of fuel on particle agglomeration

S. Banerjee and P. Sujatha Devi*
*Electroceramics Division, Central Glass and Ceramic Research Institute, Kolkata, 700 032, India; *Author for correspondence (E-mail: psujathadevi@cgcri.res.in)*

Received 6 March 2006; accepted in revised form 10 December 2006

Key words: nanocrystalline cerium oxide, mixed fuel process, thermal analysis, sintering, ceramics

Abstract

A modified combustion process, namely a mixed fuel process making use of a mixture of two fuels, such as citric acid and glycine has been developed to prepare nanocrystalline ceria powders. The effect of the mixed fuel and the different fuel to oxidant ratios on the decomposition characteristics of the gels were investigated by simultaneous thermal analysis experiments. It was established from various characterization techniques that the ceria powder prepared through the mixed fuel process has got the optimum powder characteristics, namely, a surface area of 33.33 m^2/g and a crystallite size of 14 nm compared to the powders produced through the combustion process using a single fuel like glycine or citric acid. Such powders when sintered at 1250°C resulted in pellets with densities in the range of 94–96% of theoretical density. In this paper, we have carried out systematic studies on the sintering of ceria powders prepared by different approaches. The sintered ceramic from mixed fuel batch, exhibited and retained relative density more than 95% up to 1250°C and this data clearly underscores the ability of this process in developing ceria ceramics with increased stability against reduction.

Introduction

Ceria (CeO_2) is a well-known refractory material with fluorite structure, which can accommodate both intrinsic and extrinsic oxygen vacancies and thus could act as an oxide ion conducting material. The intrinsic vacancies are formed by the presence of Ce^{3+} ions in the fluorite lattice due to the reduction equilibrium of Ce^{3+}/Ce^{4+}, whereas extrinsic vacancies arise by substitution of aliovalent ions in the lattice. These materials were studied extensively for their wide range of applications in fuel cells, sensors and in catalytic converters (Varhegyi et al., 1995; Inaba & Tagawa, 1996; Mogensen et al., 2000; Jurado, 2001; Kharton et al., 2001; Stefanik & Tuller, 2001; Cabrera et al., 2002; Li et al., 2002; Yabe & Sato, 2003; Zhang et al., 2003). The special ability of ceria to reversibly exchange oxygen is a key feature in most of its applications. As shown in Eq. (1), ceria can act as an oxygen storage material and can absorb or release oxygen in response to the oxygen partial pressure.

$$CeO_2 \leftrightarrow CeO_{2-x} + x/2\ O_2\ (g) \quad (1)$$

Various techniques are available to produce homogeneous and highly reactive nanocrystalline ceria powder at lower temperatures than the conventional methods. Wet chemical routes, such as hydrothermal synthesis (Zhou et al., 1993; Hirano

& Kato, 1996; Wu et al., 2002), mimic alkoxide method (Li et al., 2001), sol–gel technique (Chu et al., 1993), co-precipitation method (Chen & Chen, 1993; Chen & Chang, 2005), spray hydrolysis (Li et al., 2002; Xu et al., 2002), thermal hydrolysis (Hirano et al., 2000), microemulsion method (Masui et al., 1997; Zhang et al., 2001; Wu et al., 2002), electrochemical synthesis (Zhou et al., 1995), polyol method (Ho et al., 2005), alcohothermal (Zheng et al., 2005), microwave assisted synthesis (Yang et al., 2005; Fu et al., 2005), and solution combustion routes (Nakane et al., 1997; Purohit et al., 2001; Mokkelbost et al., 2004; Basu et al., 2004), are known for the synthesis of nanocrystalline ceria powders. However, most of these methods dealt only with the synthesis and characterization, and only a few further studied the sinterability of the powders. Among the available wet chemical processes, combustion synthesis has recently emerged as a highly promising powder preparation technique. This method makes use of the exothermicity of the redox reaction between oxidants such as metal nitrates and fuels such as citric acid, glycine, urea etc. Among the various combustion processes available, glycine-nitrate process (GNP) and citrate-nitrate process (CNP) are the most popular ones. CNP is a much simpler, cheaper and safer process than GNP and has recently been established as a novel technique to prepare ceramic oxides with diverse properties (Basu et al., 2004 and the references therein). Among the different advantages, low processing cost, high-energy efficiency and high production rates are noteworthy of this process.

We (Basu et al., 2004) have recently reported the synthesis of nanocrystalline ceria powder by CNP. By this process, although the sintering temperature could be lowered compared to the conventional methods, but still was substantially higher to get dense ceramics. We have modified the CNP further by a *Mixed Fuel Process* (*MFP*), which is capable of producing sinter active ceria powders that can be densified at much lower temperatures than the CNP reported by us earlier (Basu et al., 2004). The mixture of fuels used, namely citric acid and glycine together act as the dual role of effective complexing agents and fuels for favoring combustion. Though combustion process utilizing a single fuel are well established for the synthesis of ceria powder (Purohit et al., 2001; Mokkelbost et al., 2004) the same using a mixture of fuels and low cost chemicals such as ceric ammonium nitrate, citric acid and glycine is a rather new approach to prepare highly sinter active, nanocrystalline cerium oxide economically. Aruna and Rajam (Aruna & Rajam, 2004) used a mixed fuel approach to prepare Al_2O_3–ZrO_2 nanocomposite with a mixture of urea and glycine. Earlier, we have used this approach to develop sinteractive $La(Ca)CrO_3$ ceramics for SOFC applications (Kumar et al., 2004). However, the aim of this paper is to establish the novelty of this economically viable and safe process in preparing sinter active nanocrystalline ceria powders and to correlate the characteristics of the powders prepared under different conditions with their sinterability. First time, we have carried out a systematic study on the sinterability of nanocrystalline ceria powders prepared by different approaches to understand the effect of crystallite size on the stability against reduction of pure ceria powder.

Experimental procedure

Powder synthesis

All the chemicals used were of analytical reagent grade. Ceric ammonium nitrate [$(NH_4)_2[Ce(NO_3)_6$), 99% Merck Ltd. Mumbai, India] was dissolved in distilled water to form 0.2 molar stock solutions. For the synthesis of different batches calculated volume of ceric ammonium nitrate, citric acid monohydrate ($C_6H_8O_7{\cdot}H_2O$, (99.5% Merck Ltd., Mumbai, India) and glycine (99% purity, E. Merck, Mumbai, India) were added to the nitrate solution according to the compositions shown in Table 1. CIT/NIT refers to citrate to nitrate and GLY/NIT refers to Glycine to nitrate. The resulting translucent solution was heated on a hot plate with constant stirring which resulted in a viscous liquid, here after termed as precursor. On further heating, the precursor turned into a yellow-colored gel, which finally ignited with glowing flints and evolution of large volume of gases. This auto-ignition of the precursor finally resulted in the formation of voluminous yellowish white ash powders. The ash powder obtained after combustion was calcined at 300°C for 6 h resulting in light yellowish white foamy powder.

Table 1. Physical characteristics of the gel samples and their nature of decomposition

Samples ID	CIT/NIT	GLY/NIT	Color of the gel	Nature of decomposition	Color of the ash powder	Texture of ash powder
Ce0g	0.3	0	Light yellow	Moderate decomposition	Off-white	Fine and porous
Ce1g	0.0	0.05	Light orange	Very slow decomposition with fire	Yellow	Coarse and fluffy
Ce2g	0.0	0.1	White and transparent	Slow decomposition with both fire and flame	Yellow	Coarse and fluffy
Ce3g	0.3	0.05	Yellow	Rapid decomposition with controlled burning	Off-white	Fine, fluffy and porous
Ce4g	0.3	0.1	Yellow	Very fast decomposition with controlled burning	Off-white	Fine, fluffy and porous

Characterization of the precursor gel and the powder samples

The thermal decomposition studies and X-ray powder diffraction (XRD) studies on the synthesized gel and powder were performed as reported earlier by us (Basu et al., 2004). Particle size analysis of the calcined powders was carried out using a Sedigraph 5100 Micromeritics particle size analyzer. For particle size analysis, 300°C calcined powders were well dispersed in 0.5 wt.% Calgon solution. No surfactant was added to aid in the dispersion of the particles. Surface area analysis of the calcined powders was also carried out on a Micromeritics Gemini II 2370 surface area analyzer. The specific surface area (SSA) was converted into particle size assuming that the particles are closed spheres with smooth surface and uniform size (Purohit et al., 2001).

Particle size and morphology of the synthesized powders were further monitored with the help of a transmission electron microscope (TEM), JEOL (JEM-200X). The combustion-synthesized powders were cold pressed into 10 mm diameter pellets at a compaction pressure of around 20 MPa. Sintering was performed in air at 1200°C, 1250°C, 1300°C and 1350°C for 6 h. The density of the sintered samples i.e., the resultant sintered densities (d_{rs}) was determined using the Archimede's principle using kerosene as an intrusion medium. From the calculated theoretical density (d_{th}) and the resultant sintered density (d_{rs}), the relative density was calculated as $d_{rd} = d_{rs}/d_{th}$. Microstructural studies on the powder and sintered samples were carried out on a Leo 430i scanning electron microscope. For sintered bodies, the sample surface was polished to 1 μm finish with diamond paste and then thermally etched in air at a temperature 50°C lower than the sintering temperature.

Results and discussion

Physical characteristics

All the gel compositions were hygroscopic and sticky in nature and exhibited different color. The preparative conditions used for different batches and their physical characteristics are shown in Table 1.

Thermal decomposition characteristics of the gel samples

Figures 1 and 2 show the thermal analysis plots obtained for the yellow colored dried gel samples. The DTA plots of each composition exhibited an intense exothermic peak at around 225°C–300°C (Figure 1). The samples where no citric acid has been added, the DTA peak shifted to the left indicating a decrease in the decomposition temperature. Most of the samples exhibited two exothermic peaks in the DTA around 250°C–265°C and 450°C–600°C, the former indicating the decomposition temperature while the latter corresponding to the burning of the residual organic matter and subsequent crystallization of CeO_2. The sharp change in weight between 200°C and 260°C in the TGA plots (Figure 2) is a strong evidence of the single step decomposition nature of the gel. The thermal characteristics associated with the decomposition of the gel samples are tabulated in Table 2. The composition Ce0g exhibited the lowest enthalpy change and the Ce2g exhibited the highest enthalpy change. But, when a combination

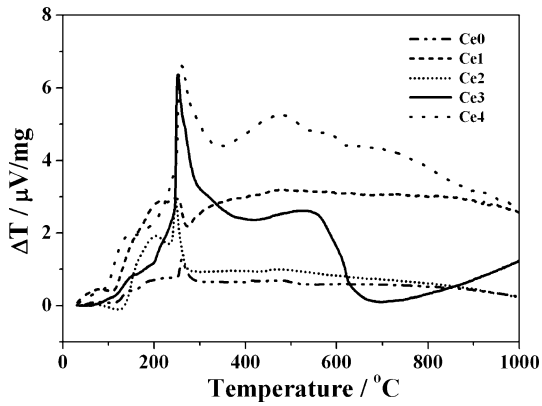

Figure 1. DTA plots of ceria gels prepared by varying the fuel to nitrate ratio.

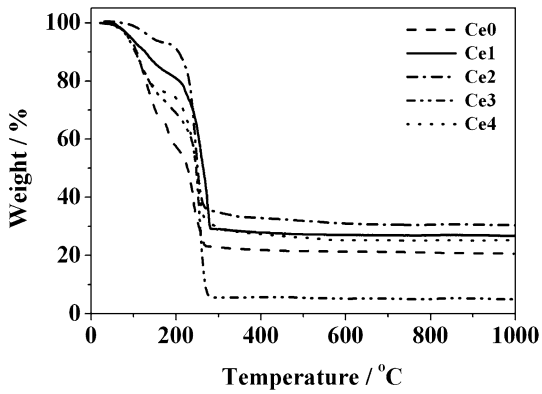

Figure 2. TGA plots of ceria gels with different fuel to oxidant ratio.

of the two fuels was used, the combustion reaction became less vigorous and controllable with ΔH coming down to −571.01 J/g. In the mixed fuel batches (Ce3 and Ce4), note however, the increased ΔH with rise in glycine content from GLY/NIT = 0.05–0.1 at a fixed CIT/NIT ratio of 0.3. The exothermicity of a combustion process is governed by the ratio of the oxidant to the fuel used for combustion. In our experiments, we have used a mixture of fuels containing citric acid and glycine together acting as a fuel for combustion. Citric acid with a heat of combustion of 10.2 kJ/g is a polyhydroxy carboxylic acid with three carboxylic acid groups and one hydroxyl group and hence could be a very good complexing agent, in addition to acting as a fuel for combustion (Hwang et al., 2004). Glycine with a higher heat of combustion of 13.0 kJ/g, also has a zwitterionic character with one carboxylic group at one end and an amino group at the other end, both of which can take part in complexation (Hwang et al., 2004). Thus, the poly functional citric acid could be a better complexing agent while glycine could be a better fuel for combustion reactions. Hence, a combination of the two fuels is expected to produce ceramic oxides with better homogeneity, phase purity and superior powder characteristics.

Based on the concept of propellant chemistry, the ratio of the oxidizing valency of the metal nitrates (O) to the reducing valency of the fuel (R) should be unity to get the maximum exothermicity during a combustion reaction. We have calculated the (O/R) ratio of oxidant to fuel for the system under investigation. The oxidizing and reducing valencies were calculated by considering the valencies of elements as +4 for Ce, +4 for C, +1 for H, −2 for O, and 0 for N. Thus the oxidizing valency for $(NH_4)_2[Ce(NO_3)_6$ is −24 and the reducing valencies for citric acid and glycine are +18 and +9, respectively.

According to the propellant chemistry, the idealized reactions that would occur during the combustion synthesis of ceria using ceric ammonium nitrate, citric acid and glycine are given below:

$$(NH_4)_2[Ce(NO_3)_6] + 8/3NH_2CH_2COOH \rightarrow CeO_2 + 16/3CO_2 + 16/3N_2 + 32/3H_2O \quad (2)$$

Table 2. Thermal characteristics of the CeO_2 precursor materials

Samples	Fuel/Nitrate (F/N) ratio	(O/R)	(%) weight loss	Decomposition temperature (T_P) (°C)	Enthalpy ΔH (J/g)
Ce0g	0.30	0.74	95.15	260.5	−146.0
Ce1g	0.05	8.88	71.11	247.9	−214.9
Ce2g	0.10	4.44	79.37	226.2	−662.05
Ce3g	0.35	0.68	70.06	253.3	−442.53
Ce4g	0.40	0.63	74.70	260.2	−571.01

$$(NH_4)_2[Ce(NO_3)_6] + 4/3C_6H_8O_7 \rightarrow CeO_2 + 8CO_2 + 4N_2 + 28/3H_2O \quad (3)$$

Adding (2) and (3) gives,

$$(NH_4)_2[Ce(NO_3)_6] + 2/3C_6H_8O_7 + 4/3NH_2CH_2COOH \rightarrow CeO_2 + 20/3CO_2 + 14/3N_2 + 10H_2O \quad (4)$$

According to Eq. (4) the optimum ratios of CIT/NIT and GLY/NIT, where the O/R will be unity to prepare CeO_2 from ceric ammonium nitrate should be 0.11 and 0.22, respectively. However, it is worth noting that we have conducted the mixed fuel process with a higher CIT/NIT ratio of 0.3 and a lower GLY/NIT ratio of 0.1 in order to slow down the vigor of the combustion reaction since the use of glycine alone has been shown to result in combustion reactions with uncontrollable flame and heat leading to local sintering of particles and formation of hard agglomerates. Previously, we have optimized the CNP with a CIT/NIT ratio of 0.3 to prepare nanocrystalline ceria powder samples (Basu et al., 2004). Purohit et al., on the other hand, carried out the glycine-nitrate combustion synthesis of CeO_2 powders with a lower, stoichiometric and higher GLY/NIT ratios and concluded that at lower ratio, auto-ignition ceases to occur whereas reaction becomes violent in case of stoichiometric and higher ratios due to the occurrence of very high flame temperature. The optimum fuel ratio we have used is turned out to be a fuel rich composition.

When only citric acid was used as the fuel, the (O/R) is equal to 0.74. Use of a small amount of glycine on the other hand increased the (O/R) value to 8.88 (Table 2). When the mixed fuel was introduced, the (O/R) value again, is lower than 1 (fuel rich). It is interesting to note the lower enthalpy change exhibited by the Ce0 batch with a higher (O/R) ratio of 0.74. The Ce4 batch with a lower (O/R) ratio of 0.634 on the other hand exhibited a substantially higher enthalpy of around −571.01 J/g, emphasizing the effect of glycine as a better fuel than citric acid for combustion process. Ce1 and Ce2 are fuel deficient compositions and Ce0, Ce3 and Ce4 are fuel rich compositions.

Characterization of the powder samples

The weight changes associated with the as-burnt ash samples are shown in Figure 3. The amount of un-burnt material present was minima in the Ce0 sample compared to others. Maximum amount of un-burnt material was retained in the ash powder produced with only glycine. The X-ray diffraction patterns of the as-synthesized and 300°C calcined powder samples are shown in Figures 4 and 5, respectively, where typical diffraction peaks of ceria are evident (JCPDS File 34-394). *In situ* formation of crystalline CeO_2 phase was confirmed from the diffraction pattern of the as-formed material (Figure 4). The XRD peaks of the as-synthesized powders are quite broad and of less intense compared to that of the 300°C calcined powder (Figure 5) reflecting the nanocrystalline nature of the as-synthesized powder. The XRD peaks became sharper and the line broadening decreased with increase in calcination temperature for all the ceria compositions. The crystallite size of both uncalcined and 300°C calcined ceria powders as calculated using Scherrer's formula are presented in Table 2. An increase in crystallite size as a function of fuel content was evident from such measurements. A comparison of the X-ray line broadening data (Figure 6) from different powders show a peak shift towards lower angles and peak broadening with decrease in crystalline size. Figure 7 shows the dependence of the calculated unit cell parameter ‚*a*' to the observed crystallite size of the as-prepared and 300°C calcined powder samples. An increase in the lattice parameter was observed with a decrease in the crystallite size. An

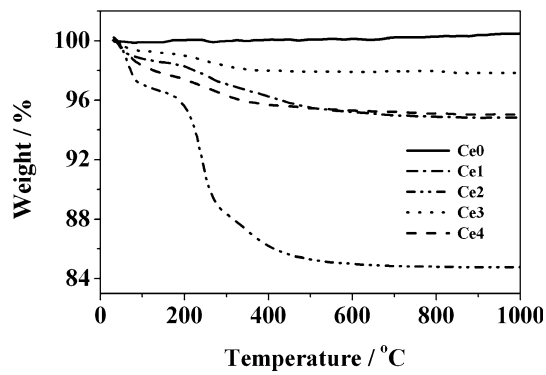

Figure 3. TGA plots of as-prepared ceria ash samples.

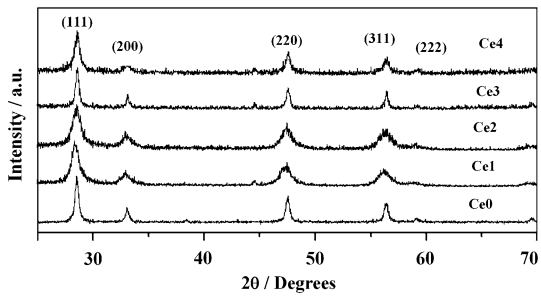

Figure 4. XRD patterns of the uncalcined powders indicating the *in situ* formation of ceria.

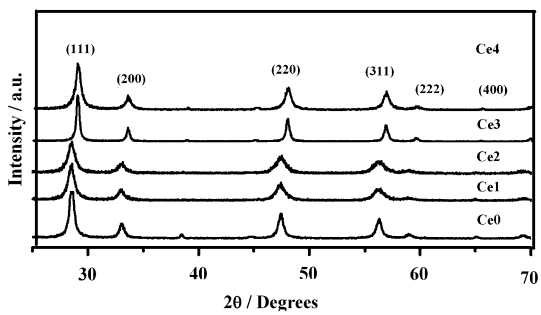

Figure 5. XRD patterns of the 300°C calcined ceria samples.

expansion of the ceria lattice with a decrease in particle size was reported earlier also by Zhang et al., where the lattice expansion has been assigned to the presence of Ce^{3+} and or oxygen vacancies. In our case also, the high reactivity of the nanoparticles would have caused the reduction of Ce^{4+} (0.97 Å) ion and consequent formation of Ce^{3+} ion with a higher ionic radii (1.14 Å). Moreover, the different colors exhibited by the uncalcined ceria powders from different batches could also be related to the variation of the crystallite size. The off-white color of the ash powders of Ce0, Ce3 and Ce4 are due to their larger crystallite sizes. On the other hand, the ash powders of Ce1 and Ce2 samples having smaller crystallite sizes of less than 10 nm were yellow in color. Yu et al. (2000) also reported a change in color of the ceria nanopowders. Studies on the catalytic and gas sensing activity of such powders are under progress.

Particle size distribution of the 300°C calcined powder is shown in Figure 8(a) and (b), respectively. The particle size and their distribution were found to depend very much on the nature of ignition of the gel. When the CIT/NIT ratio was increased from 0.0 to 0.3, the average size of the

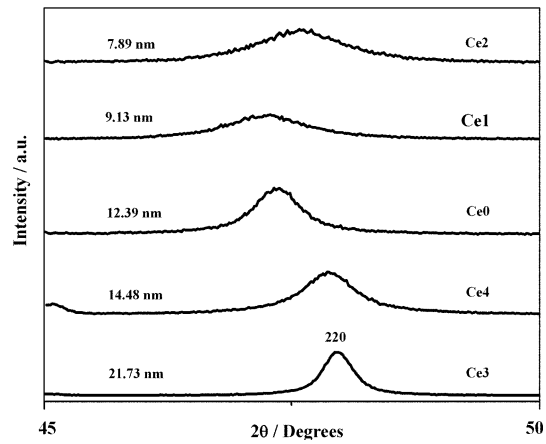

Figure 6. Effect of fuel on the line broadening of (220) reflection.

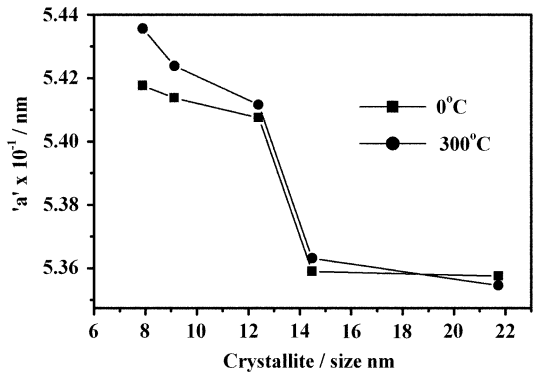

Figure 7. Data showing the effect of particle size on the lattice parameter.

particles exhibited a reduction in size from 0.50 to 0.24 μm. When glycine was introduced along with citric acid, the derived powders exhibited nearly identical size distribution with an average particle size of around 0.24–0.37 μm. From the data presented in Table 3, it is clear that the powders derived from Ce1 and Ce2 batches exhibited higher particle agglomeration whereas those prepared by mixed fuel process exhibited weaker particle agglomeration (Table 3). Independent of the fuel to nitrate i.e., (F/N) ratios used, all the samples exhibited a broader size distribution (Figure 8b). Moreover, it is also evident that Ce1 and Ce2 batches have maximum amount of particles in the 0.1–1.0 μm size range whereas others contain much finer particles. The gels of Ce3 and Ce4 where citric acid was also present

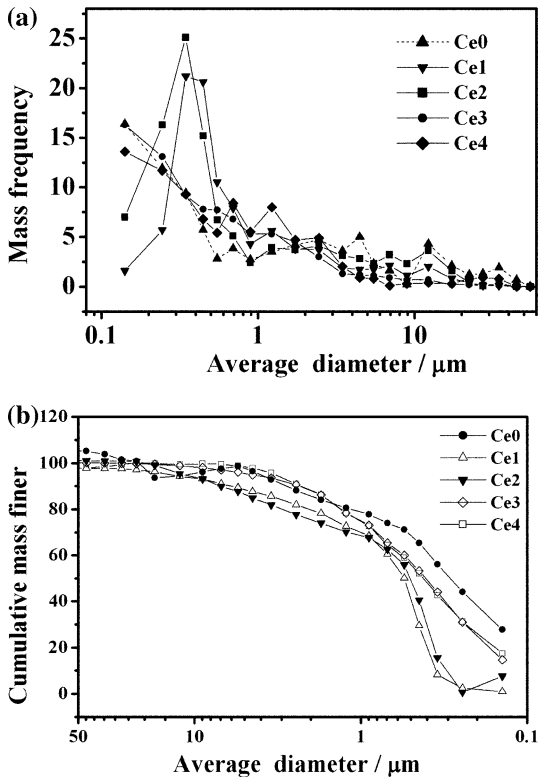

Figure 8. (a) and (b) Particle size distribution of the 300°C calcined ceria samples.

along with glycine, gives out a higher number of evolved gases, thereby dissipating the evolved heat and minimizing the local sintering making the powders less agglomerated. On the other hand, the burning of gels Ce1 and Ce2 resulted in the formation of hard agglomerates with larger particle size.

The specific surface area of the 300°C calcined powders along with corresponding average crystallite and particle sizes of all the compositions are shown in Table 3. A variation in the specific surface area of ceria powders as a function of the fuel to nitrate molar ratio was noticed. Approximately a three-fold increase in surface area was obtained by changing the fuel from mere citric acid in Ce0 to a mixture of fuels in Ce4. This increase indicates a strong influence of the fuel content used in the combustion mixture on the powder characteristics.

A large particle size calculated from surface area compared to the crystallite size measured by XRD illustrates the extent of agglomeration among the particles. The ratio of D_{BET} to D_{XRD} designated as the extent of agglomeration (Table 3) is lowest for the powder derived from Ce4 batch and highest for the powder derived from Ce0 batch. Consequently, the ceria powder derived from Ce0 batch exhibited the lowest surface area and that derived from Ce4 batch exhibited the highest surface area.

Microstructural studies on powder samples

Figure 9 shows the SEM micrograph of the 300°C calcined CeO_2 powder derived from Ce4 batch. The powder is composed of agglomerated particles with an average particle size of the order of 300–400 nm size. Figure 10(a–c) shows typical TEM micrographs of the 300°C calcined ceria samples. The 300°C calcined powder from Ce0 batch indicated the presence of large and agglomerated grains, whereas that from Ce1 batch showed the presence of fine crystallites of 10–15 nm size range. The powder derived from Ce4 composition (Figure 10c) on the other hand is comprised of a chain like arrangement of crystallites in the 20–30 nm size range.

Densification studies on the ceria powder compacts

The sintered densities were determined using Archimede's principle and the corresponding (%)

Table 3. Physico-chemical characteristics of the 300°C calcined powder samples

Samples	Color	D_{XRD} (nm)	S_{BET} (m^2/gm)	D_{BET} (nm)	Extent of agglomeration (D_{BET}/D_{XRD}) (nm)	D_{50} (μm)	Green density (g/cm^3)	d_{rs} 1250°C (g/cm^3)
Ce0	Light yellow	12.39	11.00	75.60	6.10	0.24	2.680	6.334
Ce1	Yellow	9.13	25.40	32.74	3.61	0.50	3.138	6.105
Ce2	Dark yellow	7.89	29.60	28.09	3.56	0.45	3.078	6.220
Ce3	Off-white	21.73	16.67	50.00	2.3	0.36	2.698	6.317
Ce4	Light yellow	14.48	33.33	24.95	1.72	0.37	2.547	6.928

densification at different temperatures is plotted in Figure 11. The green density and the sintered density of the ceria powder were found to be a function of the fuel content in the precursor gel. The green density of the ceria powder compacts derived from Ce1 and Ce2 was 44% of its theoretical density whereas others produced only 35–37% of theoretical density. The higher green density of Ce1 and Ce2 may be due to the presence of particles in a narrow distribution range of 0.1–1.0 μm in the powder leading to better compaction. At 1150°C for 6 h, sintering of the powders derived from Ce0, Ce3 and Ce4 exhibited almost 92.5–94.5% of relative density. It was difficult to densify the powders derived from Ce0 batch may be due to the highly agglomerated powders. Ce0 exhibited maximum density at 1150°C, which then started to decrease with increase in the sintering temperature. Maximum density of 96.03% was attained for the Ce4 powder compacts at 1250°C, whereas Ce1 and Ce2 showed very poor densification at 1250°C. The weakly and less agglomerated starting powders with a high surface area are responsible for obtaining a better densification of the Ce4 powder.

Figure 12 indicates the effect of crystallite size on the relative (%) densification of the ceria powders produced in different batches. At lower sintering temperatures i.e., $T_s \leq 1200$°C, the powders with crystallite size >14 nm exhibited a constant (%) relative densification, implying no tendency of reduction. As the temperature was raised further, powders having crystallite size >14 nm or <14 nm exhibited a reduction in the relative densification, probably due to the reduction of CeO_2 to Ce_2O_3. Thus, the powders derived from MFP with a crystallite size of around 14 nm were found to be optimum to obtain sintered densities of 96% or above. As per Herring's Scaling law, grain boundary diffusion is enhanced with decreasing particle size. Hence, the enhanced

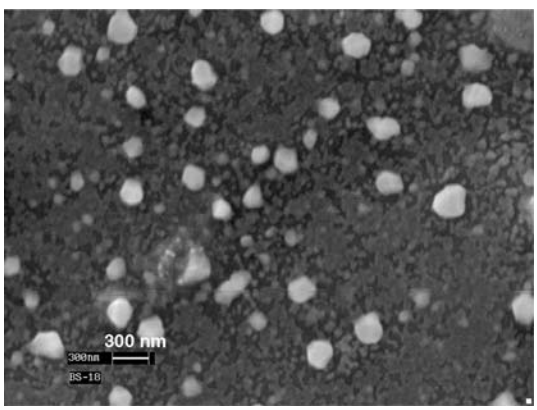

Figure 9. SEM picture of a representative Ce4 batch powder.

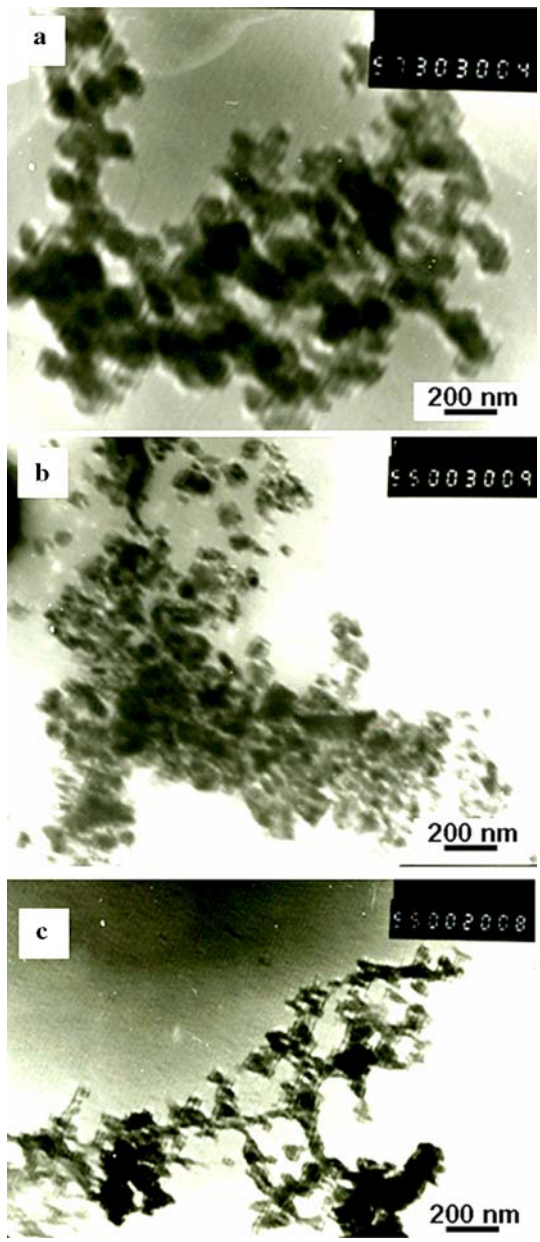

Figure 10. TEM pictures of the 300°C calcined ceria powders derived from (a) Ce0, (b) Ce1 and (c) Ce4 batches.

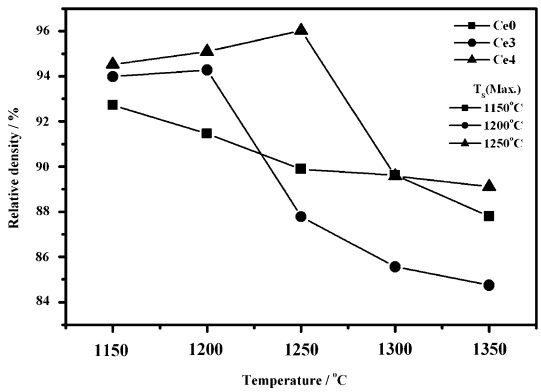

Figure 11. Variation of relative density with sintering temperature of CeO_2 powder compacts.

densification observed here could be due to the finer particles produced by the mixed fuel process.

Figure 13 indicates the variation of the (%) densification with the fuel content in the mixture. Powders derived from Ce0 batch with no glycine, exhibited a reduction in the (%) densification with temperature, as is evident from Figure 13. It is worth noting the better stability of the powders derived from Ce4 batch, i.e., (the MFP) where the sintered ceramic exhibited and retained RD more than 94% up to 1250°C and the tendency of reduction started only at 1300°C. The above data is very much suggestive of the ability of MFP in developing ceria ceramics with increased capability in restricting the CeO_2 reduction.

The sintering data shown in Figure 11 indicate that all the ceria powder compacts exhibited a decrease in density beyond the maximum sintering temperature. For example, the sintered density of Ce0 starts to decrease at 1150°C, while that of Ce3 starts to decrease at 1250°C and Ce4 at 1300°C only. This decrease in density at higher temperature is believed to be due to the reduction of CeO_2 to Ce_2O_3. According to Rahaman & Zhou (1995) and Zhou & Rahaman (1997), the above redox reaction is accompanied by the formation of an oxygen vacancy for each pair of Ce^{4+} ions being reduced, i.e.,

$$CeO_2 \rightarrow Ce_2O_3 + 1/2O_2 \tag{5}$$

$$O_o^x \rightarrow V_O + 2e' + 1/2O_2 \tag{6}$$

Thus, they also observed a reduction in the density of ultrafine ceria powders above a sintering temperature of around 1200°C (Zhou & Rahaman 1993, 1997). The samples, sintered above the maximum sintering temperature, exhibited a discoloration thereby confirming the reduction of ceria at high temperatures. The color of the sintered pellets at 1250°C varied in the order grey-yellow-yellow-darkgrey-off white for Ce0-Ce1-Ce2-Ce3-Ce4 thereby confirming the tendency of reduction. The actual mechanism of sintering of the ceria powders prepared by the combustion process is not clear at this point.

The SEM microstructures of the sintered pellet of Ce0C and Ce4 at 1150°C are shown in Figure 14. The microstructure of the 1150°C sintered Ce0 ceria powder compact is comprised of large

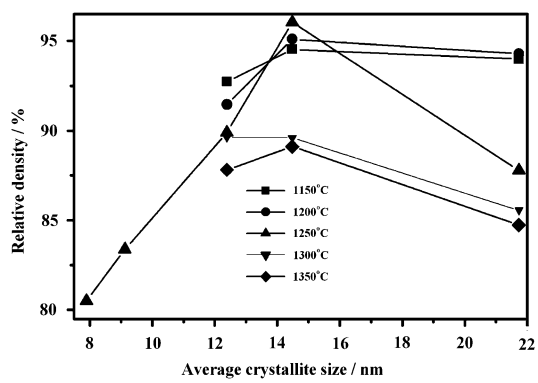

Figure 12. Effect of crystallite size on the densification behavior of ceria samples.

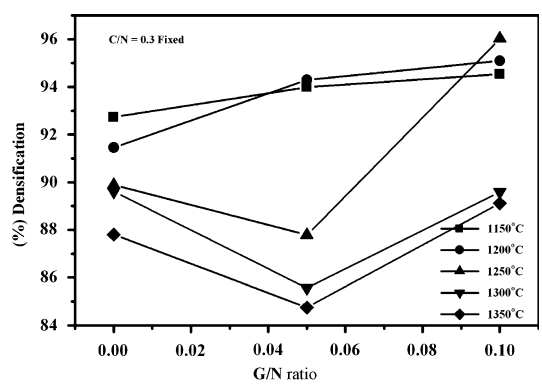

Figure 13. Effect of G/N ratio on the densification behavior of ceria powders.

intergranular pores with a high porosity, where as that derived from Ce4 batch is dense containing smaller and less number of pores. Figure 15 indicates a comparison of the microstructures of Ce0, Ce3 and Ce4 powder compacts sintered at 1200°C. Ce0 powder compact exhibited a microstructure with maximum porosity consisting of large inter and intra-granular pores. The ceramics derived from Ce3 and Ce4 batches on the other hand exhibited a dense microstructure with a bimodal grain size distribution. We believe that this difference in the grain size distribution is due to the different degree of agglomeration of particles and presence of particles with a wider range of size distribution in the starting powder. Such wider particle distribution of particles is believed to affect the initial compaction behavior and kinetics of sintering substantially.

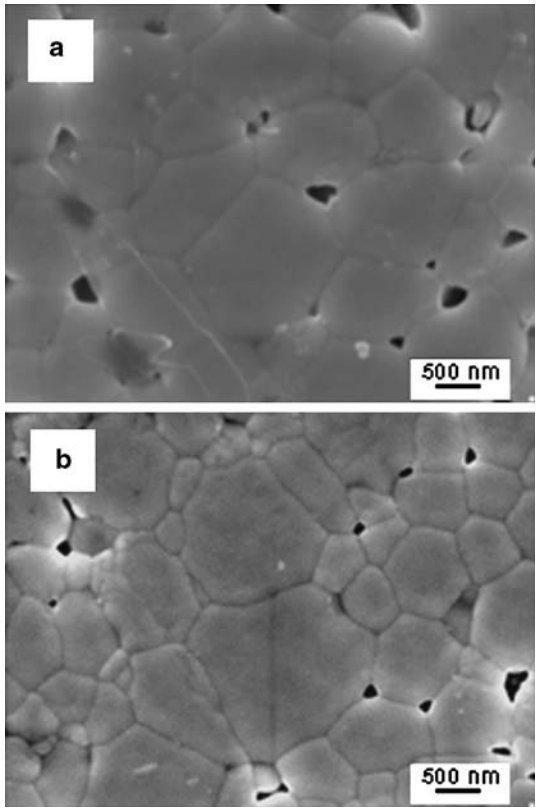

Figure 14. Microstructures of 1150°C sintered (a) Ce0 and (b) Ce4 powder compacts.

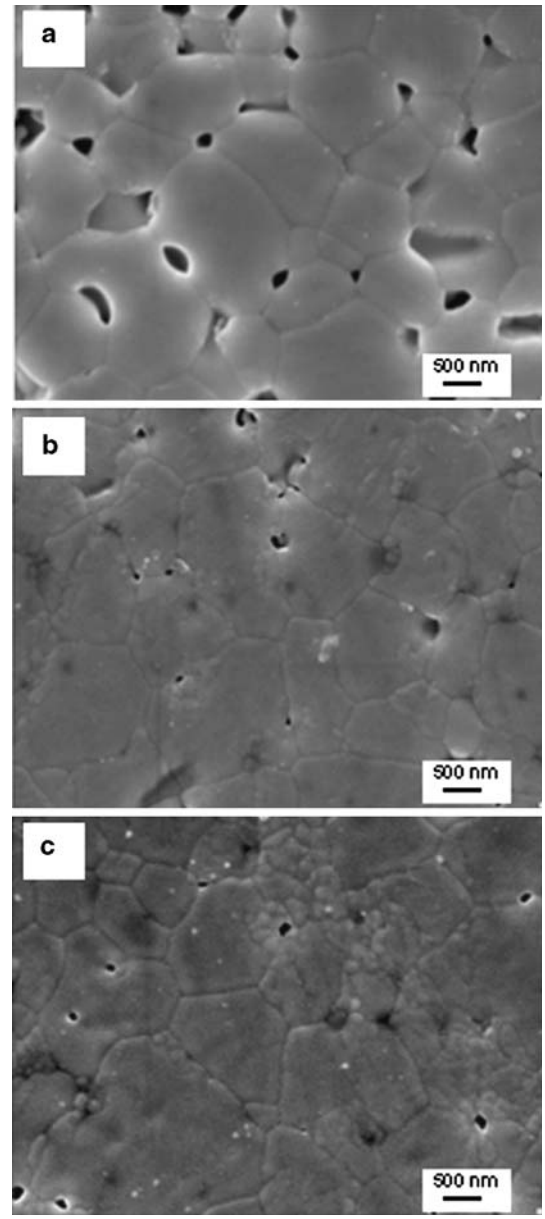

Figure 15. A comparison of the microstructures of ceria samples sintered at 1200°C (a) Ce0, (b) Ce3 and (c) Ce4.

Conclusion

In this paper, we report the synthesis, characterization and properties of nanocrystalline CeO_2 powders prepared by a modified auto ignition technique named as a mixed fuel process (MFP) using a mixture of citric acid and glycine as fuels and nitrate as an oxidizer where phase pure ceria

has been formed *in situ* during the combustion. It can be established that the ceria powder prepared through the mixed fuel process has got the optimum powder properties such as surface area 33.33 m^2/g, crystallite size 14 nm, and average agglomerate size of ~375 nm, compared to the powders produced through the combustion process using a single fuel like glycine or citric acid. Consequently, the highest sintered density was obtained for the powders derived from the mixed fuel batch. In case of the mixed fuel composition, the sintered density reached a maximum of 96% of theoretical at 1250°C and then started decreasing. In this paper, we have also carried out a systematic study on the sintering of ceria powders prepared by different approaches and evaluated the stability of the powders against chemical reduction during sintering.

Acknowledgements

The authors thank Director, Central Glass and Ceramic Research Institute for permission to publish this work. S. Banerjee is indebted to Council of Scientific and Industrial Research (CSIR) for the award of Senior Research Fellowship (SRF-NET). Technical assistance from the X-ray and SEM divisions of CG & CRI is also acknowledged. The authors also thank all the members of the Electroceramics Division of CGCRI for their cooperation at every stage of this work.

References

Aruna S.T. & K.S. Rajam, 2004. Mater. Res. Bull. 39, 157.
Basu S., P.S. Devi & H.S. Maiti, 2004. J. Mater. Res. 19(11), 3162.
Cabrera E.R., A. Atkinson & D. Chadwick, 2002. Appl. Catal. B: Environ. 36(3), 193.
Chen H.I. & H.Y. Chang, 2005. Ceram. Int. 31, 795.
Chen P.L. & I.W. Chen, 1993. J. Am. Ceram. Soc. 76, 1577.
Chu X., W. Chung & L.D. Schmidt, 1993. J. Am. Ceram. Soc. 76, 2115.
Doshi R., V.L. Richards, J.D. Carter, X. Wang & M. Krumpelt, 1999. J. Electro. Chem. Soc. 146(4), 1273.
Fu P.Y., C.H. Lin & C.S. Hsu, 2005. J. Alloys Compds. 39, 110.
Godickemeier M. & L.J. Gauckler, 1998. J. Electro. Chem. Soc. 145(2), 414.
Hirano M., Y. Fukuda, H. Iwata, Y. Hotta & M. Inagaki, 2000. J. Am. Ceram. Soc. 83, 1287.
Hirano M. & E. Kato, 1996. J. Mater. Sci. Lett. 15, 1249.
Ho C., J.C. Yu, T. Kwong, A.C. Mak & S. Lai, 2005. Chem. Mater. 17, 4514.
Hwang C.C., T.Y. Wu, J. Wan & J.S. Tsai, 2004. Mater. Sci. Eng. B 111, 49.
Inaba H. & H. Tagawa, 1996. Solid State Ionics 83, 1.
Izu N., W. Shin, N. Murayama & S. Kanzaki, 2002. Sens. Actuator B 87, 95.
Jasinski P., T. Suzuki & H.U. Anderson, 2003. Sens. Actuators B 95, 73.
JCPDS File 34-394, Nat. Bur. Stand. (U.S.) Monogr. 1983. 25, 2038.
Jurado J.R., 2001. J. Mater. Sci. 36, 1133.
Kharton V.V., F.M. Figueiredo, L. Navarro, E.N. Naumovich, A.V. Kovalevsky, A.A. Yaremchenko, A.P. Viskup, A. Carneiro, F.M.B. Marques & J.R. Frade, 2001. J. Mater. Sci. 36, 1105.
Kumar A., P.S. Devi & H.S. Maiti, 2004. Chem. Mater. 16, 5562.
Li J.G., T. Ikegami, J.H. Lee & T. Mori, 2001. Acta Mater. 49, 419.
Li R., S. Yabe, M. Yamashita, S. Momose, S. Yoshida, S. Yin & T. Sato, 2002. Mater. Chem. Phys. 75, 39.
Masui T., K. Fujiwara, K. Machida & G. Adachi, 1997. Chem. Mater. 9, 2197.
Mogensen M., N.M. Sammes & G.A. Tompsett, 2000. Solid State Ionics 129, 63.
Mokkelbost T., I. Kaus, T. Grande & M.A. Einarsrud, 2004. Chem. Mater. 16, 5489.
Nakane S., T. Tachi, M. Yoshinaka, K. Hirota & O. Yamaguchi, 1997. J. Am. Ceram. Soc. 80(12), 3221.
Purohit R.D., B.P. Sharma, K.T. Pillai & A.K. Tyagi, 2001. Mater. Res. Bull. 36, 2711.
Rahaman M.N. & Y.C. Zhou, 1995. J. Eur. Ceram. Soc. 15, 939.
Stefanik S.T. & L.H. Tuller, 2001. J. Eur. Ceram. Soc. 21, 1967.
Varhegyi E.B., J. Gerblinger, F. Reti, I.V. Perczel & H. Meixner, 1995. Sens. Actuators B 24–25, 631.
Wu N.C., E.W. Shi, Y.Q. Zheng & W.J. Li, 2002. J. Am. Ceram. Soc. 85(10), 2462.
Xu H., L. Gao, H. Gu, J. Guo & D. Yan, 2002. J. Am. Ceram. Soc. 85(1), 139.
Yabe S. & T. Sato, 2003. J. Solid State Chem. 171, 7.
Yang H., C. Huang, A. Tang, X. Zhang & W. Yang, 2005. Mater. Res. Bull. 40, 1690.
Yu X., F. Li, X. Ye & X. Xin, 2000. J. Am. Ceram. Soc. 83(4), 964.
Zhang F., S.W. Chan, J.E. Spanier, E. Apak, Q. Jin, R.D. Robinson & I.P. Herman, 2002. Appl. Phys. Lett. 80(1), 127.
Zhang J., X. Ju, Z.Y. Wu, T. Liu, T.D. Hu, Y.N. Xie & Z.L. Zhang, 2001. Chem. Mater. 13, 4192.
Zhang Y.W., R. Si, C.S. Liao & C.H. Yan, 2003. J. Phys. Chem. B 107, 10159.
Zheng X., S. Wang, X. Wang, S. Wang, X. Wang & S. Wu, 2005. Mater. Lett. 59(22), 2769.
Zhou Y.C., R.J. Philips & J.A. Switzer, 1995. J. Am. Ceram. Soc. 78, 981.
Zhou Y.C. & M.N. Rahaman, 1993. J. Mater. Res. 8(7), 1680.
Zhou, Y.C. & M.N. Rahaman, 1997. Acta Mater. 45(9), 3635.